DEFORMATION-MECHANISM MAPS AND THE CREEP OF TUNGSTEN LAMP FILAMENTS

H. J. Frost, et al

Harvard University

Prepared for:

Office of Naval Research

October 1972

Office of Naval Research
Contract N00014-67-A-0298-0020 NR-031-732

DEFORMATION-MECHANISM MAPS AND THE CREEP OF TUNGSTEN LAMP FILAMENTS

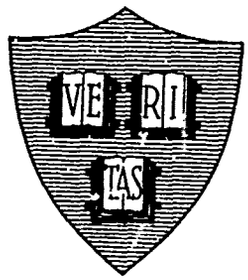

By

H. J. Frost and M. F. Ashby

October 1972

Technical Report No. 7

Division of Engineering and Applied Physics
Harvard University • Cambridge, Massachusetts

37

Unclassified
Security Classification

DOCUMENT CONTROL DATA - R & D

Security classification of title, body of abstract and indexing annotation must be entered when the overall report is classified)

1 ORIGINATING ACTIVITY (Corporate author) Division of Engineering and Applied Physics Harvard University Cambridge, Massachusetts 02138	2a. REPORT SECURITY CLASSIFICATION Unclassified 2b GROUP

3 REPORT TITLE

DEFORMATION-MECHANISM MAPS AND THE CREEP OF TUNGSTEN LAMP FILAMENTS

4 DESCRIPTIVE NOTES (Type of report and, inclusive dates)

Interim technical report

5 AUTHOR(S) (First name, middle initial, last name)

H. J. Frost
M. F. Ashby

6 REPORT DATE	7a. TOTAL NO OF PAGES	7b. NO OF REFS
October 1972	37	8

8a CONTRACT OR GRANT NO	9a. ORIGINATOR'S REPORT NUMBER(S)
N00014-67-A-0298-0020 b PROJECT NO NR-031-732	Technical Report No. 7
c d	9b. OTHER REPORT NO(S) (Any other numbers that may be assigned this report)

10 DISTRIBUTION STATEMENT

This document has been approved for public release and sale; its distribution is unlimited. Reproduction in whole or in part is permitted by the U. S. Government.

11 SUPPLEMENTARY NOTES	12 SPONSORING MILITARY ACTIVITY
	Office of Naval Research

13 ABSTRACT

A crystalline solid can deform plastically in a number of ways. Deformation mechanism diagrams can be constructed which display the fields of stress and temperature in which a given mechanism is dominant, and the strain rate it yields. This report describes some refinements in the computation of the diagrams, and illustrates their use by means of a case-study: the creep of tungsten lamp filaments.

ig

DD FORM 1 NOV 65 1473 (PAGE 1)
S/N 0102-014-6700

Unclassified
Security Classification

D-23822

14 KEY WORDS	LINK A		LINK B		LINK C	
	ROLE	WT	ROLE	WT	ROLE	WT
Plastic flow						
Deformation mechanisms						
Dislocation glide						
Dislocation creep						
Diffusional flow						
Nabarro-Herring creep						
Coble creep						

16

Office of Naval Research

Contract N00014-67-A-0298-0020

NR-031-732

DEFORMATION-MECHANISM MAPS AND THE CREEP OF TUNGSTEN LAMP FILAMENTS

By

H. J. Frost and M. F. Ashby

Technical Report No. 7

October 1972

The research reported in this document was made possible through support extended the Division of Engineering and Applied Physics, Harvard University, by the Office of Naval Research, under Contract N00014-67-A-0298-0020.

Division of Engineering and Applied Physics

Harvard University · Cambridge, Massachusetts

ic

DEFORMATION-MECHANISM MAPS AND THE CREEP OF TUNGSTEN LAMP FILAMENTS

By

H. J. Frost and M. F. Ashby

Division of Engineering and Applied Physics

Harvard University, Cambridge, Massachusetts

ABSTRACT

A crystalline solid can deform plastically in a number of ways. Deformation mechanism diagrams can be constructed which display the fields of stress and temperature in which a given mechanism is dominant, and the strain rate it yields. This report describes some refinements in the computation of the diagrams, and illustrates their use by means of a case-study: the creep of tungsten lamp filaments.

PART I: DEFORMATION-MECHANISM MAPS.

A. INTRODUCTION

A crystalline solid can deform plastically in a number of different ways. It can deform by dislocation glide alone; by glide plus climb (dislocation creep); by diffusional flow of matter through its grains (Nabarro-Herring creep) or around its grain boundaries (Coble creep); by mechanical twinning; and by combinations of these and other mechanisms. To a first approximation each mechanism may be considered to operate independently of the others, and to be capable of permitting steady-state flow. Each has a particular dependence on stress and temperature and will therefore dominate the deformation over a particular, characteristic, range of stress and temperature.

This rather complicated behavior can be presented on a map with axes of stress and temperature (Ashby, 1972). The map is divided into *fields* which indicate the regions of stress and temperature where each of the various mechanisms are dominant, as shown in Fig. 1. Superimposed on the fields are *contours of constant strain-rate*: these show the net strain-rate, due to appropriate superposition of all the mechanisms that a given combination of stress and temperature will produce. The map depicts the relationship between three variables: stress, temperature, and strain-rate. If any two of these variables are specified, the map can be used to determine the third.

A deformation map is constructed by using the *rate-equation* (which relates stress, temperature, and strain-rate) for each of the mechanisms. This involves assumptions about the way in which the mechanisms interact. It is easiest to assume that all mechanisms operate independently and that the strain-rates produced by each can be added together to give the total resultant strain-rate: on this basis, the formula which yields the greatest strain-rate at a given stress-temperature point will determine which mechanism is dominant. With

slight restrictions, this method produces surprisingly good results, because for most areas one particular mechanism formula dominates dramatically. (In fact, we have made a slightly more sophisticated assumption, to be discussed below.) Once the equations and method of superposition are specified, the map can be constructed easily by a computer program.

All the maps shown here have a linear temperature scale, normalized with respect to the melting temperature, and a logarithmic stress scale, normalized with respect to the shear modulus. This permits a logical comparison of the flow behavior of materials. Normalized in this way, maps for FCC metals, for instance, form a group: they are broadly similar to each other, but differ significantly from those for BCC metals, or diamond cubic materials, which constitute separate groups. All the maps are plotted in terms of equivalent shear-stress, τ, and shear strain-rate, $\dot{\gamma}$, since this allows their application to complex stress states. These are related to the tensile stress σ and strain-rate $\dot{\varepsilon}$ by $\tau = \sigma/\sqrt{3}$ and $\dot{\gamma} = \sqrt{3}\ \dot{\varepsilon}$.

A major value of the maps is that they provide a means to present and visualize the complicated relations between different deformation mechanisms. They are also a useful means to compare experiment with theory. In the center of a field an experiment should fit well with the dominant mechanism. Near a field boundary we would expect behavior representing a combination of mechanisms. Finally, the maps provide a qualitative way for choosing a material for engineering applications, for predicting the mechanisms by which it deforms, and hence in selecting, or predicting the effects, of strengthening mechanisms; an example of such an application is presented as a Case Study in Part II of this paper.

B. RATE EQUATIONS

The maps presented in this paper are based on mechanisms:

1) Dislocation Glide

   a) Limited by Peierls stress.

   b) Limited by discrete obstacles.

2) Dislocation Creep

   a) High Temperature Creep.

   b) Low Temperature Creep.

3) Diffusional Creep

   a) Nabarro-Herring Creep (volume diffusion)

   b) Coble Creep (grain boundary diffusion)

Consider now the rate equations for each of these mechanisms.

1. Dislocation Glide. At low temperatures (less than 1/3 T_m, where T_m is the absolute melting temperature) the deformation is dominated by the *glide motion of dislocations*. For the strain-rate produced by glide we have used equations based on the thermal activation of dislocations over short-range barriers, either due to a Peierls resistance, or to discrete obstacles. This approach greatly simplifies what is theoretically a very complex situation, but the resulting equations give a reasonable fit with experiment.

In a complete description, the strain-rate depends on how quickly the dislocations overcome the barriers to their glide and how quickly they move from one barrier to the next. Under most conditions the dislocations move relatively quickly from one barrier to the next, and the strain-rate can be adequately described in terms of the waiting time spent at barriers. At strain-rates higher than any which interest us here, the limit on the free velocity of the dislocation imposed by phonon and other drags does become important. But for the rates shown in the diagrams of this paper such effects play no role; we have ignored them.

Barriers to dislocation glide can be divided into various classes (see, for example, Kocks et.al., 1973). In particular, we can distinguish between barriers that can be overcome with the aid of thermal activation and those that cannot (*thermal* and *athermal* barriers respectively). Typical examples of athermal barriers are long-range stress fields and incoherent precipitates; solute atoms, or a Peierls resistance typify thermal barriers. We may further distinguish different types of thermally activatable barriers. In this paper we have considered two of these: *localized obstacles* (forest dislocations), and a *Peierls potential barrier*.

In pure FCC and HCP metals the dislocations glide easily without any appreciable Peierls resistance. The flow stress can then be best described in terms of localized obstacles such as forest dislocations. Under these conditions the flow stress at absolute zero is proportional to $\frac{\mu b}{\ell}$, where ℓ is the obstacle spacing, μ is the shear modulus, and b is the Burgers vector. The constant of proportionality is complicated, depending on the strength of the obstacles and on the statistics of their distribution. We have simply used $\tau_0 = \frac{\mu b}{\ell}$ for this value. At higher temperatures part of the energy necessary to overcome an obstacle can be supplied by thermal activation. The amount of energy required by activation can be assumed to be $\Delta F\ (1 - \tau/\tau_0)$, where ΔF is the total energy required. (This is equivalent to the assumption of a square form for the strength-distance curve of the obstacle.) If we assume that the strain-rate is proportional to the frequency of activation we obtain:

$$\dot{\gamma}_1 = \dot{\gamma}_0 \exp\ \left[-\frac{\Delta F}{kT}(1 - \tau/\tau_0)\right]$$

where $\dot{\gamma}_0$ is an appropriate pre-exponential term.

Like most of the equations in this paper, this equation is based

on a model which is physically sound, but which is insufficiently precise to predict useful values of the constants ($\dot{\gamma}_0$, ΔF and τ_0). Theory gives us the *form* of the equation; we have to resort to experimental data to obtain the *physical constants* which enter it. This approach of "model inspired phenomenology" * is a powerful one in dealing with phenomena too complicated to model exactly. In particular, an equation obtained in this way can be used to extrapolate outside the range for which data is available; a purely empirical equation cannot.

The three physical constants of egn.(1) have well defined meanings. τ_0 is the flow stress at 0°K. For pure FCC or HCP metals, τ_0 describes the state of whork-hardening: at the level of approximation with which we are concerned here, ℓ can be thought of as the spacing of forest dislocations. In the computations described below, we chose ℓ to give the observed saturation flow stress (a typical value of ℓ is $10^{2}b$). The quantity ΔF is the total Helmholtz free energy required to cut an obstacle: in this case, a forest dislocation: roughly $\frac{\mu b^3}{5}$. It determines the temperature-dependence of the flow stress. Finally, $\dot{\gamma}_0$ sets the absolute magnitude of the strain-rate. Its value is not critical, since it does not enter the exponential. The value 10^{6}/sec fits experimental observations tolerably well.

Dislocation motion in BCC and diamond cubic crystals, and in oxides and carbides, is more difficult. There is a resistance to motion produced by the crystal lattice itself. This Peierls resistance increases rapidly with decreasing temperature. Following Guyot and Dorn (1967) we have used a Peierls potential of parabolic form, such that the activation energy required

---

* A term suggested by Dr. U. F. Kocks, private communication.

to move a dislocation has the form:

$$U = 2U_k \left(1 - \tau/\tau_0\right)^2$$

Here τ_0, as before, is the flow stress at absolute zero and U_k is the energy of formation of a kink pair. The strain-rate is given by $\dot{\gamma}_2$ where

$$\dot{\gamma}_2 = \dot{\gamma}_p \exp\left[-\frac{U}{kT}\right]$$

and $\dot{\gamma}_p$ is an appropriate pre-exponential term. Like the equation for obstacle-controlled glide, which it closely resembles, the constants τ_0, U_k, and $\dot{\gamma}_p$ are found by matching experiment.

Strengthening mechanisms must be distinguished from deformation mechanisms. The two strengthening mechanisms just described are obviously *not* independent mechanisms giving additive strain-rates. Their superposition is complicated; for the purposes of this paper it is sufficient to assume that the strain-rate due to dislocation glide is equal to the smaller of equations (1) and (2). Among metals, the Peierls resistance is important only for those with a BCC structure.

2. Dislocation Creep. At temperature above half the melting temperature there is sufficient mobility of vacancies to allow dislocations to *climb as well as glide*. Deformation is possible at a lower stress than would be needed for glide alone. The steady-state creep rate for high temperatures and moderate stresses can be described by the semi-empirical equation:

$$\dot{\gamma}_3 = A' \frac{D_{eff}\,\mu\, b}{kT} \left(\tau/\mu\right)^n$$

where A' and n are material constants, D_{eff} is a diffusion coefficient (usually the lattice diffusion coefficient, D_v), and the other factors are as defined above. This equation has a reasonable theoretical basis, as has been discussed by Muhkerjee, Bird, and Dorn (1969). (We have converted it from its usual tensile stress--tensile strain-rate form into an equivalent

shear stress-shear strain-rate form by using $A' = (\sqrt{3})^{n+1} A$.) Dislocation climb is limited by the diffusion of vacancies to or from the dislocation. This is reflected in the linear dependence on the diffusion coefficient. The power dependence on (τ/μ) has not been conclusively explained. Empirically, the value of n is usually between 3 and 7.

We have also included an additional dislocation creep term. At lower temperatures, transport of matter via dislocation core diffusion contributes significantly to the overall diffusive transport of matter, and may even become the dominant transport mechanism. Robinson and Sherby (1969) have suggested, rightly, we believe, that this might explain the lower activation energy for creep at lower temperatures. We have incorporated the *contribution of core diffusion* by defining an effective diffusion coefficient

$$D_{eff} = D_v f_v + D_c f_c$$

where D_c is the core diffusion coefficient, and f_v and f_c are the fractions of atom sites associated with each type of diffusion. The value of f_v is essentially unity. The value of f_c is determined by the dislocation density, ρ, as $f_c = a_c \rho$, where a_c is the cross-sectional area of the dislocation core in which fast diffusion is taking place. Experimentally it is only possible to measure the quantity $a_c D_c$. The rather sparse measurements of it have recently been reviewed by Balluffi (1970): the diffusion enhancement varies with dislocation orientation (being perhaps 10 times larger for edges than for screws), and with the degree of dissociation and therefore the arrangement of the dislocations. Even the activation energy is not constant. In general D_c is about equal to D_b, the grain boundary diffusion coefficient, if a_c is taken as about $5b^2$. By using the common experimental observation that $\rho \approx \frac{10}{b^2} (\tau/\mu)^2$ our effective diffusion coefficient becomes

$$D_{eff} = D_v \left[1 + \frac{10a_c}{b^2} (\tau/\mu)^2 \frac{D_c}{D_v}\right]$$

which is inserted into equation (3).

3. Diffusional Creep. *Diffusional flow of atoms,* either by volume diffusion or by grain-boundary diffusion, leads to the Newtonian-viscous creep of a polycrystal. The two alternative flow paths represent independent, additive contributions to the overall strain-rate. The most recent re-analysis of this problem yields the following combined constitutive equation (Raj and Ashby, 1971):

$$\dot{\gamma} = 42 \frac{\tau\Omega}{KTd^2} D_v \left\{1 + \frac{\pi\delta}{d} \frac{D_b}{D_v}\right\}$$

Here Ω is the atomic volume, d is the grain size, and δ is the effective thickness of a boundary for diffusional transport. The volume diffusion term is known as *Nabarro-Herring creep;* the boundary term is known as *Coble creep.*

4. Defect-less Flow. In addition to the mechanisms described above, we have considered the possibility of *defect-less flow.* At a sufficiently high stress (the "ideal shear strength") even a perfect, dislocation-free crystal will deform. This stress is shown as a dashed line on the maps. Its value has been calculated and refined repeatedly, (see, for example, Kelly 1966); the result is always about $\mu/20$. We have considered the temperature dependence of the ideal shear strength and find it is too small to be of importance here.

5. Other Mechanisms. Mechanical twinning does not, at present, appear on the diagrams because no usable rate-equation is available to describe it. For FCC metals it is rarely important because it only occurs at very low temperatures, typically below 20°K. Some HCP metals twin above room temperature; and twinning also may be important for BCC metals at lower temperatures.

C. CONSTRUCTION OF THE MAPS.

Dislocation creep ($\dot{\gamma}_3$) and diffusional flow ($\dot{\gamma}_4$) are independent flow mechanisms involving different defects. At a first approximation, they superimpose linearly, that is, their strain-rates add. Dislocation creep ($\dot{\gamma}_3$) and glide ($\dot{\gamma}_1$ or $\dot{\gamma}_2$) do not. Both processes involve the same defect; they describe the different behavior of dislocations under different conditions. As the stress is raised, the gliding part of the motion of a dislocation becomes more important, and the climbing part less important, until, when the boundary between the two fields is reached, climb is not necessary at all. We have solved the problem by treating dislocation creep and glide as alternative mechanisms, choosing always the faster one. (It could be argued that this choice maximizes the rate at which the free energy of the system decreases, or at which its entropy increases.) Finally, the problem of the superposition of strengthening mechanisms (mechanisms 1 and 2) was discussed earlier: as a first approximation, the slowest one is rate controlling.* In summary, the net strain-rate of a polycrystal subject to a stress τ at a temperature T is:

$$\dot{\gamma}_{net} = \dot{\gamma}_4 + \text{Greatest of } \left\{ \begin{array}{c} \dot{\gamma}_3 \\ \text{Least of } \dot{\gamma}_1 \text{ and } \dot{\gamma}_2 \end{array} \right\} \qquad (5)$$

Within a field, one contribution to eq.(5) is larger than any other. (Remember that $\dot{\gamma}_4$ and $\dot{\gamma}_3$ each describe the sum of two additive contributions.) A *field boundary* is defined as the set of values of τ and T at which a switch of dominant mechanism occurs. The *contours of constant strain-rate* are obtained by solving eq.(5) for τ as a function of T at constant $\dot{\gamma}$.

*The entire problem of the superposition of flow mechanisms and of strengthening mechanisms is a complicated one which we are at present attempting to refine.

These operations can only be performed by digital computation. The way we have done it involves the use of a subroutine EQNS shown in the Appendix, which evaluates eq.(5) incrementally for 50 temperature increments and 80 logarithmically spaced increments of stress (these chosen to allow plotting of the results on the line printer), and which identifies the dominant mechanism.

The position of a strain-rate contour is bracketed by searching over stress increments until one increment yields a strain-rate lower than the contour value, and the next a strain-rate higher than the contour value. Similarly, the field boundaries are located by finding the neighboring stress increments where the dominant mechanism changes. The search for strain-rate contours for the first temperature increment is done by searching upward through stress increments one at a time, locating the contours as they are passed. For all their temperature increments the search for a particular contour starts at the stress level of that contour for the previous temperature increment. During this search, the dominant mechanism at each point calculated by EQNS is stored. This information is then used in a search for the mechanism field boundaries, along with additional calling on EQNS for points not calculated in the strain-rate contour search. Quantities such as the diffusion coefficients and the shear modulus, which vary with temperature, are evaluated in the main program and transfered to the subroutine.

D. DISCUSSION.

Two examples of deformation maps are given in Fig. 1. They are for pure nickel with grain sizes of 10 and 1000 microns. There is a large region on the maps at low stresses and low temperatures where the behavior is essentially elastic. The rate-equations can be used to predict strain-rates in

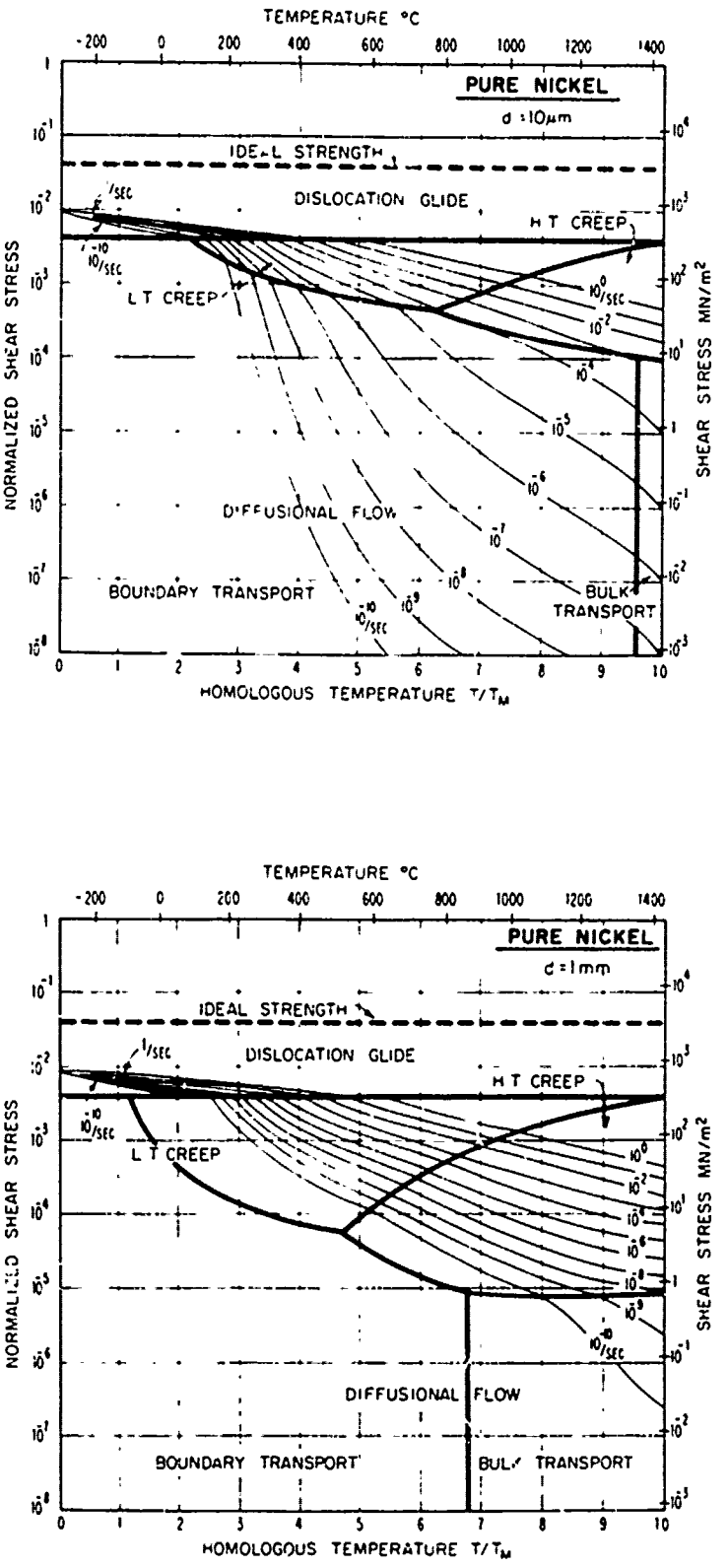

Fig. 1. Deformation maps for pure nickel of grain size 10μm and 1mm.

this region, but the values are far too low to be observed experimentally. The extent of the elastic region depends on the choice of the minimum observable strain-rate; we chose 10^{-10}/sec.

The *stress-dependence* of any mechanism is reflected in the vertical spacing of the strain-rate contours. Mechanisms with greater dependence on stress will dominate at higher stresses, as is shown by the positions of dislocation and diffusional creep. Similarly, the *temperature-dependence* of any mechanism is shown by the horizontal spacing of the strain-rate contours. The temperature dependence of both diffusional and dislocation creep results primarily from the diffusion coefficient. High temperature dislocation creep and Nabarro-Herring creep have the same dependence on D_v and the boundary between them is therefore a line of constant stress. The same is approximately true of the boundary between Coble creep and low temperature dislocation creep. There *is* a definite temperature dependence in the glide region, but it is made less prominent by the logarithmic stress scale.

The *effect of grain size* in these maps is confined to the diffusional creep fields. The Nabarro-Herring creep-rate is proportional to d^{-2}, and the Coble creep-rate is proportional to d^{-3}. This means that these fields will expand into the dislocation creep fields as the grain size is decreased. We have not included any grain-size dependence in the dislocation-creep region. There may be some grain-size effect in this region, especially when the grain size is small: comparable to the dislocation cell size, but this is poorly characterized, and in most cases is not very important. Experimentally there is often a grain-size dependence in the glide region, typically following the Hall-Petch relation, the flow stress (at a given γ) varying as $d^{-\frac{1}{2}}$. This we have omitted because we assumed that the glide behavior is characterized

by either a Peierls stress or by a sufficient density of obstacles to overshadow the grain-size effect.

The most obvious limitation of the maps in their present form is their *limitation to steady-state flow.* Time- and strain-dependent effects are not included. One can construct maps using time or strain-dependent constitutive equations, though displaying the results in a useful way is difficult.

The assumption of steady-state flow is quite adequate for diffusional creep. At least in pure metals, the defect structure (vacancy concentration, dislocation density) does not change with time. This is the sense in which we use the term "steady-state". The overall state of the polycrystal may change: the grain shape and grain boundary area, and the external surface area, may change. These changes do, in fact, alter the response of the polycrystal to stress, but the effect is almost always trivially small. Operationally, the material behaves as if at steady state.

The assumption of steady-state flow is acceptable for dislocation creep. Most materials present a well defined steady-state secondary creep-rate in the appropriate range of temperature and stress. This steady-state behavior continues until either necking or internal cavitation sufficiently changes the structure to bring on tertiary creep. The primary creep behavior of a metal can vary depending on the processing history. From the viewpoint of the recovery--work hardening theories of creep, the transient primary is a period of work-hardening (or recovery) that the metal undergoes until it reaches the steady-state microstructure that is appropriate for the given stress and temperature. The constitutive equation we use for dislocation creep assumes that the metal is in that state. This means that we assume a different structure (microstructure) for every point in the dislocation creep

field.

The assumption of steady-state flow is least accurate for dislocation glide. Low temperature experiments produce work-hardening and yield point phenomena. The closest approximation to steady-state glide is at saturation work-hardening, at which the work-hardening rate has dropped to zero. In tensile tests this state is not usually achieved because necking intervenes first. It is mechanically possible, however, in compression or torsion tests. To approximate it we have used high obstacle densities in the obstacle controlled glide equation.

It is not necessary to describe the glide region in terms of saturation work-hardening. If a glide equation is used that describes the temperature and strain-rate dependence of a yield stress, then the glide region describes a different sort of phenomenon (non-steady-state flow) than the creep regions (steady state). The boundary between glide and dislocation creep then depends on strain or time; a given diagram refers to a particular point on the stress-strain curve of the material.

Fracture has been ignored in constructing the maps. At low temperatures many materials become brittle and will fracture in tension at a lower stress than that needed for flow. This means that the low temperature glide region may be accessible only to tests carried out under high hydrostatic pressure (eg. the standard hardness test). Creep rupture may also cause confusion. If internal cavities form in a material before it enters secondary creep, then it may exhibit a minimum creep-rate that does not represent a true steady-state. Dynamic recrystallization, too, can complicate the measurement of steady-state creep rates. It typically occurs at high temperatures and small grain sizes, and is accompanied by an increase in the creep-rate

which (apparently) is the reappearance of transient creep.

A final word of caution. The diagrams shown here and in Part II are the best we can construct at present. They are only as good as the data (Table 3) and equations used to construct them. Both are still poor. The diagrams can be used for guidance but should not at present be treated as exact.

PART II: CASE STUDY. THE CREEP OF TUNGSTEN LAMP FILIAMENTS.

A. INTRODUCTION

The coiled filiament of a tungsten lamp creeps during service. This creep causes the filiament to sag, and, if it proceeds too far, causes failure by the shorting or overheating of neighboring turns of the coil. We shall here examine the mechanism by which tungsten filiaments deform in service, and the design of filiaments to avoid failure by creep.

B. STRAIN-RATE AND STRESS ON FILIAMENTS IN SERVICE

The filiament of a typical 25 or 40 watt lamp is a single-coiled, doped, tungsten wire. The dimensions of a 40 watt lamp are given in Fig. 2. Low wattage lamps like these burn at a filiament-temperature of 2250 to 2500°C, with an average life-time of about 1000 hours. (Higher-powered lamps run at higher temperatures: up to 2765°C for ordinary lamps and up to 3160°C for photo-flood bulbs -- their life can be as short as 3 hours.)

A lamp may fail in one of several ways. Most fail because evaporation from the filiament surface, or the formation of a bubble or void within it, locally reduces the cross-section producing a hot-spot, accelerated evaporation, and finally melting. The fact that most fail in this way, and not by creep, is because design against creep failure is adequate. What factors enter this design problem? To answer this question we must first consider failure by creep.

The most probable mechanism of failure by creep is illustrated in Fig. 3. A typical coil before creep is shown at (a); its dimensions for two sizes of lamp are listed in Table 1. Lamps normally burn with the

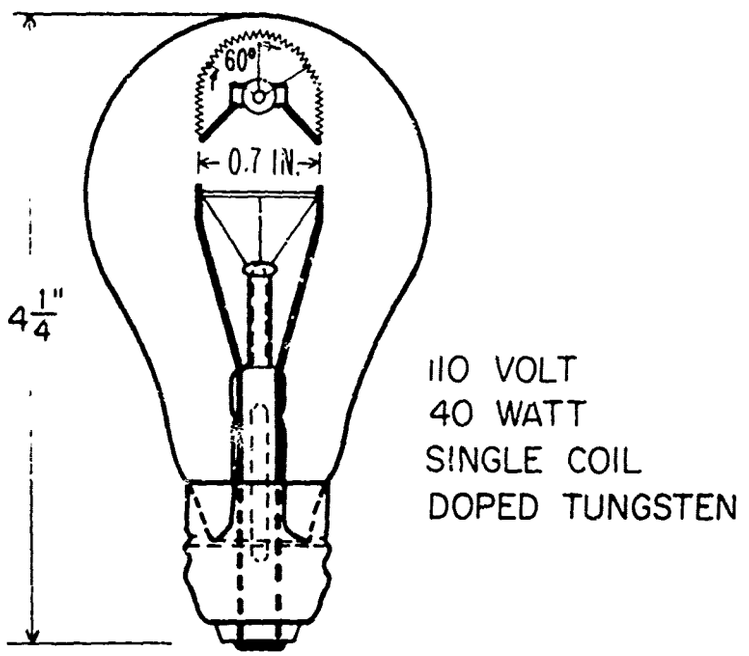

Fig. 2. A typical 40 watt, 110 volt lamp.

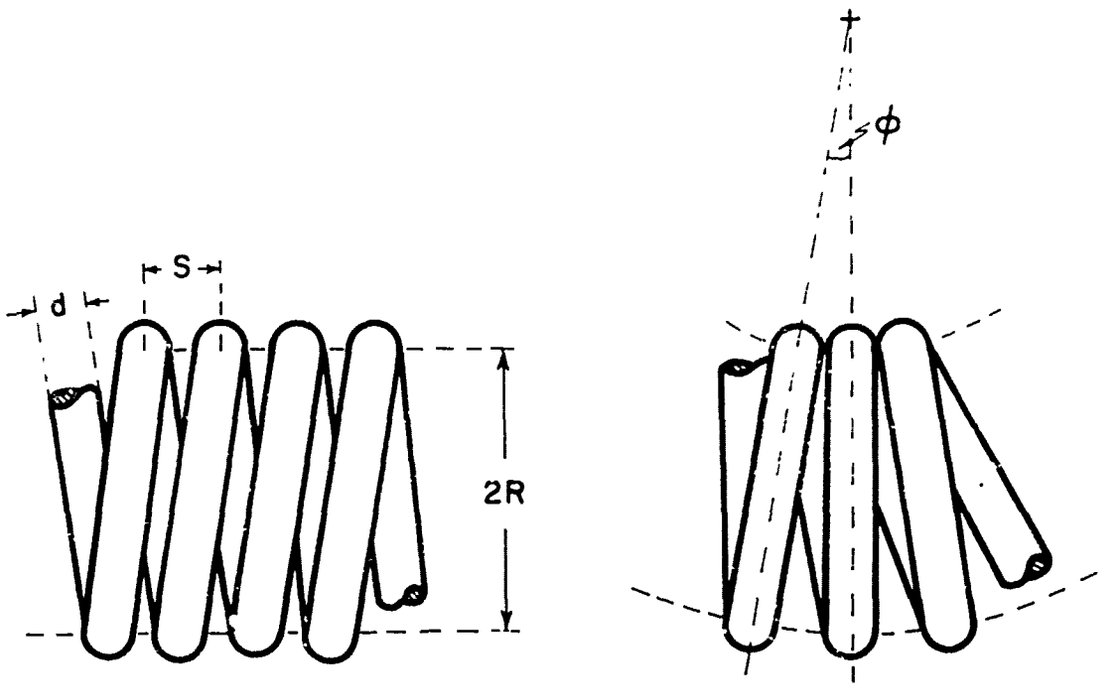

Fig. 3. The geometry of a single-coil filiament before and after creep.

filiament horizontal. Then sag by torsional creep of the wire leads to overheating, and ultimately to shorting between turns as shown at (b). Suppose elements of wire on the upper side of the coil suffer a torsional creep strain resulting in a twist of θ per unit length; those on the bottom suffer a similar twist in the opposite sense. Then the change of angle between the turns, ϕ is approximately

$$\phi = 2R\theta$$

where R is the coil radius. Contact occurs when

$$\phi R = S - d$$

where S is the turn spacing and d the wire diameter (see the figure). The shear strain at the surface of an element of the wire, γ_{MAX}, is related to the twist per unit length by

$$\gamma_{MAX} = \frac{\theta d}{2}$$

The maximum permissible strain before shorting occurs is therefore

$$\gamma_{MAX} = \frac{d(S - d)}{4R^2}$$

If the lamp is to survive its rated life-time, t, then the maximum permissible steady-state creep rate is given by

$$\gamma_{MAX} = \frac{d(S - d)}{4R^2 t}$$

Inserting data from Table 1 gives for these maximum permissible rates:

$\dot{\gamma}_{MAX} = 2.5 \times 10^{-3}$/sec 25 Watt

$\dot{\gamma}_{MAX} = 3.9 \times 10^{-9}$/sec 40 Watt

To ensure failure does not occur by creep, a maximum strain-rate of under

TABLE 1: TYPICAL LIGHT BULB SPECIFICATIONS

LAMP	BURNING TEMP (°C)	DESIGN LIFE (HOURS)	TURNS/INCH T.P.I.	TURN SPACING S (INCHES)	WIRE DIAMETER d (INCHES)	COIL DIAMETER 2R (INCHES)	TOTAL LENGTH OF WIRE (INCHES)	TOTAL LENGTH OF COIL (INCHES)	TOTAL MASS OF COIL (mg)
25 WATT SINGLE COIL	2250 - 2350	1000	670	1.5×10^{-3}	1.2×10^{-3}	6.0×10^{-3}	26	1.6	9.2
40 WATT SINGLE COIL	2400 - 2500	1000	600	1.7×10^{-3}	1.4×10^{-3}	5.6×10^{-3}	17	1.6	7.2

	NUMBER OF INTERMEDIATE SUPPORTS
25 WATT SINGLE COIL	3
40 WATT SINGLE COIL	3

10^{-9}/sec is desirable.

The shear stress on the filiament is calculated to a sufficient approximation as follows. Consider the equilibrium of a section of the coil of length ℓ between the two supports, as shown in Fig. 4. If the mass per unit length of the coil is m_0, then the length ℓ between a pair of supports requires a force $m_0 g\ell$ to support it. The upper side of each turn of the coil is then subject to a torque T, where

$$T \sim 1/2\ m_0 g\ell^2$$

The coil sags as the wire deforms plastically under this torque. We define the mean shear stress in the wire, $\bar{\tau}$, by

$$\bar{\tau} \int_0^{d/2} 2\pi r^2 dr = T$$

from which

$$\frac{\bar{\tau}}{\mu} = \frac{6m_0 g\ell^2}{\pi\mu d^3}$$

The resulting stress for the coils described here, together with the operating temperature, is shown in Table 2.

TABLE 2

	Max mean stress $\frac{\bar{\tau}}{\mu}$	Operating temp $\frac{T}{T_M}$
25 Watt	1.0×10^{-4}	.685 - .712
40 Watt	6.2×10^{-5}	.725 - .752

Summary of section B. Filiaments creep under their own weight. The design of the filiaments studied here subjects sections of the filiament

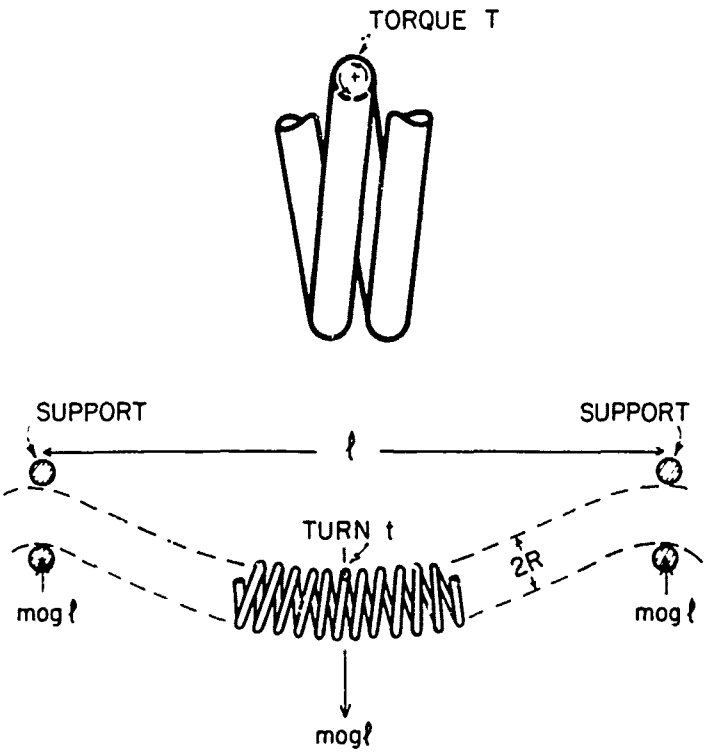

Fig. 4. The torque acting on a turn of the filiament.

coil to *normalized shear stresses* of magnitude between 6×10^{-5} and 10^{-4}, at a *homologous temperature* of between 0.68 and 0.75. To survive for the design life of 1000 hours, the *maximum steady-state creep-rate* in these filiaments must be less than 10^{-9}/sec.

C. MATERIALS CONSIDERATIONS: DEFORMATION MAPS FOR TUNGSTEN AND DOPED TUNGSTEN

Most filiaments are made from *doped tungsten:* tungsten doped with Al_2O_3, SiO_2 and K_2O (or mixed oxides of these three metals) which gives the wire added creep strength.

Microstructurally, doping introduces a fine dispersion of bubbles. This seems to have two important effects. First, it stabilizes an elongated, highly interlocked, grain structure, of a sort which cannot be obtained in pure tungsten: the grains have one dimension of order 1 mm, even in fine wires. (Such a structure cannot be obtained in fine wires of pure tungsten). Second, and independent of the grain shape, it inhibits dislocation creep.

These effects become obvious when deformation maps for pure and doped tungsten are compared. The maps shown as Figures 5, 6, and 7 were constructed using the data given in Table 3.

Consider first the maps for pure tungsten (Fig. 5). At low stresses the material deforms by *diffusional flow*; that is by Nabarro-Herring creep at the higher temperatures, and Coble creep at the lower temperatures. At higher stresses the material deforms by *dislocation creep* (also known as high temperature, or Weertman creep). In the same stress range, but at lower temperatures the material deforms by a variant of Weertman creep, in which the principal transport mechanism is by dislocation-core diffusion. At yet higher stresses, the material deforms by classical dislocation glide. Due

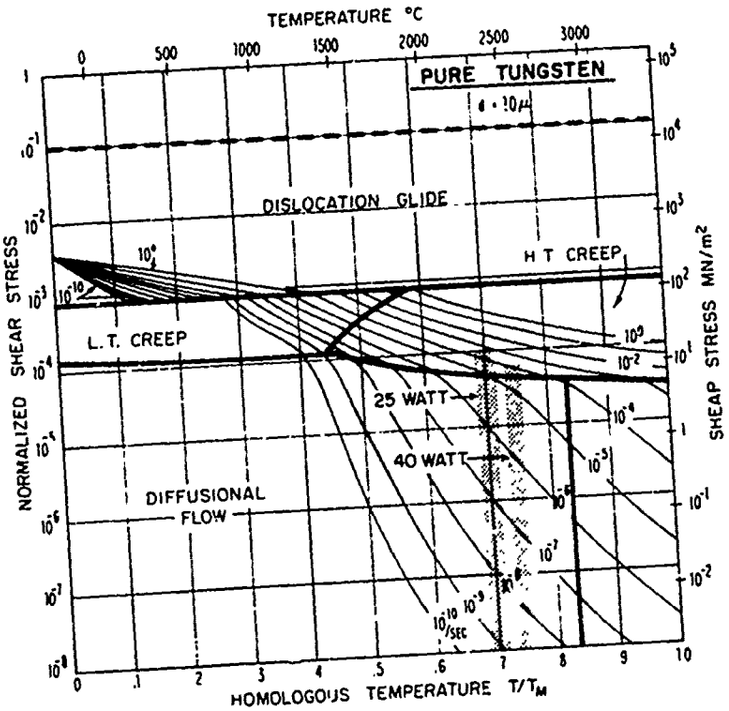

Fig. 5. A deformation map for pure tungsten of grain size 10μm. The shaded boxes show the range of stress and temperature within which the filiaments operate.

to the lattice resistance, or Peierls stress, the flow stress rises as absolute zero is approached.

Increasing the grain size from 10 microns to 1 mm (Fig. 6) expands the size of the Nabarro-Herring creep field and also of the dislocation creep field. This is simply because the larger grain size inhibits diffusional flow, but inhibits the Coble creep variety of diffusional flow more effectively than the Nabarro-Herring variety because of its more rapid grain-size dependence. Note that the application of a strengthening mechanism for diffusional flow (the change of grain size) has side effects: it expands the dislocation creep fields downwards. A specimen stressed at $2 \times 10^{-4}\ \mu$ previously deformed by diffusional flow; it now deforms by dislocation creep.

Consider now the map for doped tungsten (Fig. 7). Doping does not significantly change the yield stress (i.e. the boundary between dislocation creep and glide). But it has a profound effect on dislocation creep, greatly reducing the size of the field.

Summary of section C. Sufficient data exists to construct deformation maps for tungsten and doped tungsten. Doping stabilizes an elongated grain structure (which inhibits diffusional flow) and, independently, slows down dislocation creep.

D. CONCLUSIONS: THE CREEP MECHANISM OF FILIAMENTS

The information summarized in Table 2 can be plotted onto the maps as a box (see Fig. 5, 6, and 7). The box is defined by the range of temperature and stress to which a filiament is subjected.

Suppose first that the filiaments were made from pure, fine-grained tungsten (Fig. 5). The maximum creep rate (top of the box) would be about

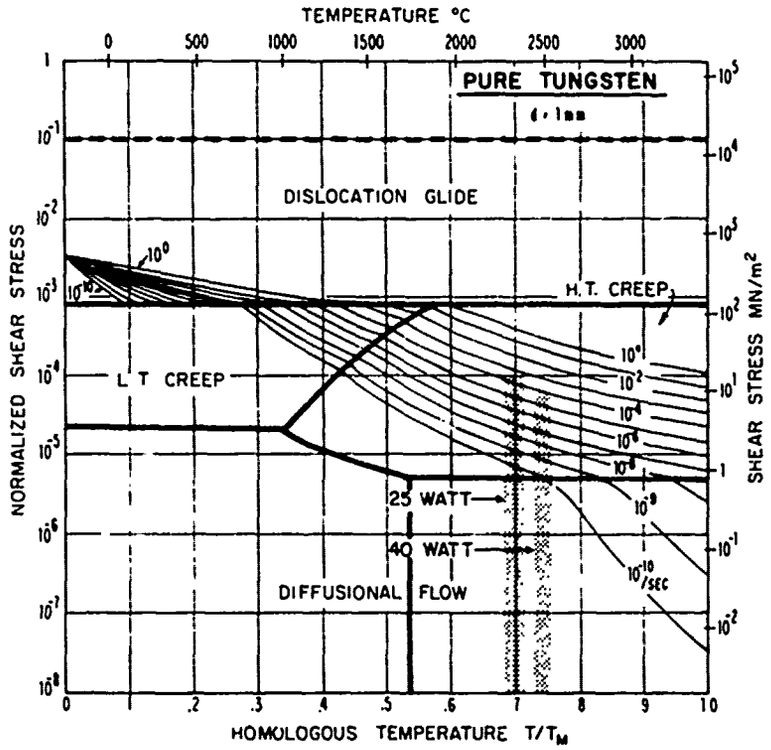

Fig. 6. Pure tungsten with a large grain size (1mm)

10^{-4}/sec: the filiament would fail by creep in 10^{-2} hours, or about half a minute. Since the mechanism giving this rate is high temperature creep, expanding the grain size (Fig. 6) does no good.

If, instead, the filiaments are made from doped tungsten (Fig. 7), then the maximum creep rate will be about 4×10^{-10}/sec, comfortably below the limit (10^{-9}/sec) required for adequate life. Furthermore, the dominant creep mechanism has been changed by doping: it is now diffusional creep.

Figure 7 can be used as a guide for filiament design. It gives guidance in determining the maximum filiament load for a given life, and allows the increase in creep rate with burning temperature to be read off.

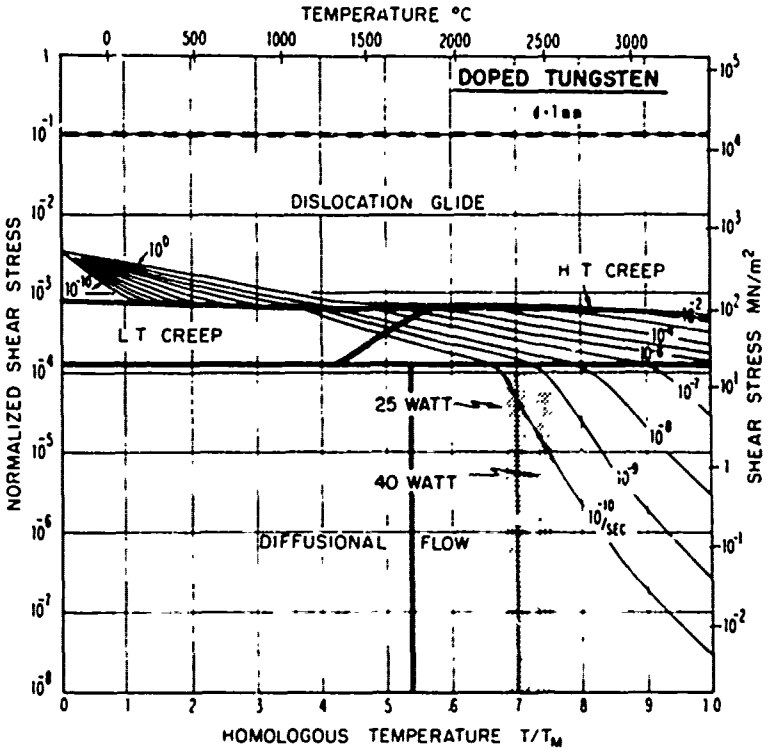

Fig. 7. Doped tungsten. In wires made of doped tungsten the grains are elongated; their long dimension can be as great as 1mm. For that reason a grain size of 1mm has been used here.

TABLE 3

		Pure Nickel	Pure (Arc-Melted) Tungsten	Doped Tungsten
Ω	Atomic Volume, cm^3	1.09×10^{-23}	1.53×10^{-23}	
b	Burgers Vector, cm	2.49×10^{-8}	2.74×10^{-8}	
T_M	Melting Point, °K	1726	3683	
μ_o	Shear Modulus at 300°K, dynes/cm^2 *	7.89×10^{11} (1)	1.55×10^{12} (5)	
$\frac{1}{\mu}\frac{d\mu}{dT}$	Temperature Dependence of Modulus, dynes/cm^2 °K	3.7×10^{-4} (1)	1.04×10^{-4} (6)	Same as for Pure Tungsten
D_{ov}	Volume Diffusion, cm^2/sec †	1.9 (2)	5.6 (7)	
Q_v	Volume Diffusion, kcal/mole	66.8 (2)	140.0 (7)	
D_{oB}	Boundary Diffusion, cm^2/sec †	0.07 (2)	3.13 (8)	
Q_B	kcal/mole	27.4 (2)	92.0 (8)	
δ	Grain Boundary Thickness, cm	5×10^{-8} (2)	1.0×10^{-7} (8)	
D_{oc}	Dislocation Core Diffusion, cm^2/sec †	3.1 (3)	10.0 (7,8)	
Q_c	kcal/mole	40.6 (3)	90.5 (8)	
A_c	Core Cross-section Area, cm^2	10^{-15} (3)	3.0×10^{-15} (13)	
n	Constants of Dorn Eq.	4.6 (4)	5.8 (4)	8.43 (12)
A	dimensionless	2.56×10^5 (4)	2.0×10^{12} (4)	8.48×10^{14} (12)
ℓ	Obstacle Spacing, cm	3.0×10^{-6} (13)	3.0×10^{-5} (9)	3.0×10^{-5}
τ_p	Peierls Stress, dyne/cm^2	--	1×10^{10} (10)	1×10^{10} (10)
U_K	Activation Energy (ergs) for Double Kink Formation	--	1×10^{-12} (11)	1×10^{-12} (11)

* $\mu(T) = \mu_o\left(1 - \frac{1}{\mu}\frac{d\mu}{dT}(T - 300)\right)$

† $D_v = D_{ov} \exp\left(-\frac{Q_v}{kT}\right)$; $D_B = D_{oB} \exp\left(-\frac{Q_B}{kT}\right)$; $D_c = D_{oc} \exp\left(-\frac{Q_c}{kT}\right)$

TABLE 3 References

(1) G. A. Alers, J. R. Neighbours, and H. Sato, J. Phys. Chem. Solids 13, 40, 1960.

(2) Ahmed Rassem Wazzan, J. Appl. Phys. 36, 3596, 1965.

(3) R. F. Canon and J. P. Stark, J. Appl. Phys. 40, 4361 (1969), 40, 4366 (1969).

(4) A. K. Mukherjee, J. E. Bird and J. E. Dorn, Trans ASM 62, 155, (1969).

(5) H. B. Huntington, Solid State Physics 7, 213, (1958).

(6) P. E. Armstrong and H. L. Brown, Trans. Met. Soc. AIME 230, 962, (1964).

(7) S. L. Robinson and O. D. Sherby, Acta Met. 17, 109 (1969).

(8) K. G. Kreider and G. Bruggeman, Trans. Met. Soc. AIME 239, 1222, (1967).

(9) G. King, private communication.

(10) Derived from P. L. Raffo, J. Less-Common Metals 17, 133, (1969).

(11) Derived from R. M. Rose, D. P. Ferriss, and J. Wulff, Trans. TMS AIME 224, 981, (1962).

(12) D. Moon and R. Stickler, Proc. 2nd International Conference on the Strength of Metals and Alloys, Asilomar, (1970); and to be published in Met. Trans.

(13) Assumed Value.

References

1. Ashby, M. F., Acta Met, 20, 887, 1972.
2. Balluffi, R. W., Phys. Stat. Sol. 42, 11, (1970).
3. Guyot, P. and Dorn, J. E., Cam. J. Phys. 45, 983 (1967).
4. Kelly, A., "Strong Solids", Oxford University Press (1966).
5. Kocks, V. F., Argon, A. and Ashby, M. F., (1973), to appear in Prog. Mat. Sci.
6. Mukherjee, A. K., Bird, J. E. and Dorn, J. E., Trans. Am. Soc. Metals, 62, 155, (1969).
7. Raj R. and Ashby, M. F., Trans. Met. Soc. AIME 2, 1113, (1971).
8. Robinson, S. L. and Sherby O. D., Acta Met. 17, 109, (1969).

Acknowledgements

This work was supported in part by the Advanced Research Projects Agency under Contract DAHC15-67-C-0219, in part by the Office of Naval Research under Contract N00014-67-A-0298-0020, and by the Division of Engineering and Applied Physics, Harvard University. One of us (H. J. F.) wishes to acknowledge the financial support of a Kennecott Copper Corp. Fellowship.

We wish to thank G. King and H. Sell of Westinghouse Lamp Division, Bloomfield, N. J. for numerous helpful discussions.

APPENDIX

```
      SUBROUTINE CONSTNEQN,NGEQN,G,GAMMA,JFIELD,T,TAU,BOLTZ,ATVOL,
     1 BURGV,SHMOD,DVOL,DBORY,DCORE,DELTA,ACORE,DGRAIN,A,EN,GAMZRO,
     2  DELF,TOBST,TAUPLS,GAMPLS,UK,TAUG)
      DIMENSION G(7)
C
C  SYMBOLS USED.
C
C  NEQN   = INTEGER WHICH SPECIFIES WHICH EQUATION SET IS TO BE USED.
C  NGEQN  = INTEGER WHICH SPECIFIES THE NUMBER OF MECHANISMS USED.
C
C  T      = TEMPERATURE
C  TAU    = SHEAR STRESS
C  BOLTZ  = BOLTZMANS CONSTANT
C  ATVOL  = ATOMIC VOLUME
C  BURGV  = BURGERS VECTOR
C  SHMOD  = SHEAR MODULUS
C  DVOL   = VOLUME DIFFUSION COEFFICIENT
C  DBORY  = GRAIN BOUNDARY DIFFUSION COEFFICIENT
C  DCORE  = DISLOCATION CORE DIFFUSION COEFFICIENT
C  DELTA  = GRAIN BOUNDARY THICKNESS
C  ACORE  = CROSS-SECTIONAL AREA OF DISLOCATION CORE
C  DGRAIN = GRAIN SIZE
C  EN     = STRESS EXPONENT IN DISLOCATION CREEP EQUATION
C  A      = DIMENSIONLESS CONSTANT FOR DISLOCATION CREEP EQUATION
C  GAMZRO = PRE-EXPONENTIAL FOR OBSTACLE CONTROLLED GLIDE
C  DELF   = ENERGY REQUIRED FOR OBSTACLE CUTTING
C  TOBST  = NORMALIZED ABSOLUTE ZERO FLOW STRESS, OBSTACLE CONTROLLED GLIDE
C  TAUPLS = NORMALIZED ABSOLUTE ZERO FLOW STRESS, PEIERLS CONTROLLED GLIDE
C  GAMPLS = PRE-EXPONENTIAL FOR PEIERLS CONTROLLED GLIDE
C  UK     = ENERGY OF KINK FORMATION
C  TAUG   = LOW STRESS CUT -OFF OF GLIDE CALCULATIONS
C  C1,C2,C3,X,Y,Z = INTERMEDIATE VALUES USED IN CALCULATIONS.
C
C  G(1) = DIFFUSIONAL CREEP RATE, NABARRO-HERRING AND COBLE TOGETHER.
C  G(2) = HIGH TEMPERATURE DISLOCATION CREEP RATE
C  G(3) = LOW TEMPERATURE DISLOCATION CREEP RATE.
C  G(4) = GLIDE STRAIN RATE.
C  THIS NUMBERING DIFFERS FROM THE NUMBERING USED IN THE TEXT.
C  GOBST  = GLIDE STRAIN-RATE FROM OBSTACLE CALCULATION.
C  GPLS   = GLIDE STRAIN-RATE FROM PEIERLS CALCULATION.
C
C  GAMMA  = NET RESULTANT STRAIN-RATE.
C  MFIELD = INTEGER WHICH SPECIFIES WHICH MECHANISM IS DOMINANT.
C
      GO TO (100,200,300,400,500), NEQN
C
C              FIRST EQNS SET,  NO PEIERLS STRESS
  100 IF(T.EQ.TLAST) GO TO 120
      X = 42.*DVOL*SHMOD*ATVOL/(BOLTZ*T*DGRAIN**2)
      C1   = X*(1.+3.1415*DELTA*DBORY/(DGRAIN*DVOL))
      C2   = (DVOL*SHMOD*BURGV/(BOLTZ*T))*A*1.732**(EN+1.)
      C3 = (10.*ACORE/BURGV**2)*(DCORE/DVOL)
      TLAST = T
  120 G(1) = C1 * TAU
      G(2) = C2 * TAU**EN
      G(3) = G(2) * C3 * TAU**2
      IF(TAU.LT.TAUG) G(4) = 0.0
      IF(TAU.LT.TAUG) GO TO 2000
      X = DELF*(1.-TAU/TOBST)/(BOLTZ*T)
      IF(X.GT.140.) X = 140.
      IF(X.LT.-140.) X = -140.
      G(4) = GAMZRO * EXP(-X)
      G23 = G(2) + G(3)
      IF(G(4).GT.G23) G(3) = 0.
      IF(G(4).GT.G23) G(2) = 0.
      IF(G(4).LE.G23) G(4) = 0.
      GO TO 2000
C
C              SECOND EQNS SET,  WITH A PEIERLS STRESS.
  200 IF(T.EQ.TLAST) GO TO 220
      X = 42.*DVOL*SHMOD*ATVOL/(BOLTZ*T*DGRAIN**2)
      C1   = X*(1.+3.1415*DELTA*DBORY/(DGRAIN*DVOL))
      C2   = (DVOL*SHMOD*BURGV/(BOLTZ*T))*A*1.732**(EN+1.)
      C3 = (10.*ACORE/BURGV**2)*(DCORE/DVOL)
      TLAST = T
  220 G(1) = C1 * TAU
      G(2) = C2 * TAU**EN
      G(3) = G(2) * C3 * TAU**2
      IF(TAU.LT.TAUG) G(4) = 0.0
      IF(TAU.LT.TAUG) GO TO 2000
      X = DELF*(1.-TAU/TOBST)/(BOLTZ*T)
      IF(X.GT.140.) X = 140.
      IF(X.LT.-140.) X = -140.
      GOBST = GAMZRO * EXP(-X)
      X = TAU*SHMOD/TAUPLS
      IF(X.GE.1.0) GO TO 240
      Y = -2.0*UK*(1.-X)**2/(BOLTZ*T)
      IF(Y.LT.-140.) Z = EXP(-140.)
      IF(Y.GE.-140.) Z = EXP(Y)
      GPLS = Z * GAMPLS
      GO TO 250
  240 GPLS = GAMPLS
  250 CONTINUE
      G(4) = AMIN1(GOBST,GPLS)
      G23 = G(2) + G(3)
      IF(G(4).GT.G23) G(3) = 0.
      IF(G(4).GT.G23) G(2) = 0.
      IF(G(4).LE.G23) G(4) = 0.
      GO TO 2000
C
  300 GO TO 2000
  400 GO TO 2000
  500 GO TO 2000
 2000 GAMMA = 0.0
      GM = 0.0
      DO 1000 J=1,NGEQN
      GAMMA = GAMMA + G(J)
      IF(G(J).GT.GM) JFIELD = J
      IF(G(J).GT.GM) GM = G(J)
 1000 CONTINUE
      RETURN
      END
```